

Performance of the GridPix detector quad

C. Ligtenberg^a, Y. Bilevych^b, K. Desch^b, H. van der Graaf^a, M. Gruber^b, F. Hartjes^a, K. Heijhoff^{a,b}, J. Kaminski^b, P.M. Kluit^a, N. van der Kolk^a, G. Raven^a, L. Scharenberg^b, T. Schiffer^b, S. Schmidt^b, J. Timmermans^a

^a*Nikhef, Science Park 105, 1098 XG Amsterdam, The Netherlands*

^b*Physikalisches Institut, University of Bonn, Nussallee 12, 53115 Bonn, Germany*

Abstract

A gaseous pixel readout module with four GridPix chips, called the quad, has been developed as a building block for a large Time Projection Chamber (TPC) readout plane. The quad module has dimensions $39.6\text{ mm} \times 28.38\text{ mm}$ and an active surface coverage of 68.9%. The four GridPix chips each consist of a Timepix3 chip with integrated amplification grid and have a high efficiency to detect single ionisation electrons, which enable it to make a precise energy loss (dE/dx) measurement. A quad module was installed in a small TPC and measurements of 2.5 GeV electrons were performed at the ELSA accelerator in Bonn, where a silicon telescope was used to provide a reference track. The error on the track position measurement, both in the pixel plane and drift direction, is dominated by diffusion. The quad was designed to have minimum electrical field inhomogeneities and distortions, achieving systematics of better than $13\text{ }\mu\text{m}$ in the pixel plane. The resolution of the setup is $41\text{ }\mu\text{m}$, where the total systematic error of the quad detector is $24\text{ }\mu\text{m}$.

Keywords: Micromegas, gaseous pixel detector, micro-pattern gaseous detector, Timepix, GridPix, time projection chamber

1. Introduction

2 In drift chambers charged particles are identified through ionisation in the
3 gas. For the readout of a Time Projection Chamber (TPC) the finest granu-
4 larity is offered by pixel readouts. In particular, a GridPix is a CMOS pixel
5 readout chip with an integrated amplification grid added by MEMS postpro-
6 cessing techniques [1, 2]. As a result, single ionisation electrons can be detected
7 with great precision, allowing an estimate of the number of clusters for an energy
8 loss (dE/dx) measurement for particle identification.

9 The original GridPix using the Timepix chip [3] has recently been succeeded
10 by the GridPix based on the Timepix3 chip [4]. This newer chip offers superior
11 timing, faster readout speed and the possibility to apply time walk corrections.
12 The first results of a single chip detector have been analysed and published in [5].

Diffusion was found to be the dominant error on the track position measurement and systematics in the pixel plane remained below $10\ \mu\text{m}$. Using a truncated sum, an energy loss (dE/dx) resolution of 4.1 % was found for an effective track length of 1 m. The single chip detector was operated reliably in a test beam experiment. However, equipping a large detector surface poses an entirely new challenge.

In order to cover a large detector surface, it is practical to subdivide it into a number of standardized modules. Here we present the design of the four chip quad module. Because the quad module has all services under the active area, it can be tiled to cover arbitrarily large areas. The performance of a TPC read-out by a single quad module was tested at the ELSA test beam facility in Bonn. Possible applications are in TPCs at future electron-positron colliders, other particle physics experiments and medical imaging such as proton therapy [3, 6].

2. Quad detector design and construction

2.1. The Timepix3 based GridPix

Here the GridPix consists of a Timepix3 chip with an integrated grid. Directly on the surface of the Timepix3 chip, a $4\ \mu\text{m}$ thick Silicon-rich Nitride protection layer is deposited in order to prevent damage to the readout chip from discharges. On top of this $50\ \mu\text{m}$ high SU8 pillars are attached that support the $1\ \mu\text{m}$ thick aluminium grid that has $35\ \mu\text{m}$ diameter circular holes aligned to the pixel input pads. The grid and dykes mask was reoptimized: at four sides the grid ends on a solid SU8 dyke for which on two sides three readout columns were sacrificed. The Timepix3 chip has low noise ($\approx 70\ e^-$) and allows for a simultaneous measurement of the Time of Arrival (ToA) and the Time over Threshold (ToT) using a TDC (clock frequency 640 MHz) per pixel. For the readout, one out of the eighth available links per chip is connected to a SPIDR board [7] at a speed of 80 Mbps. The hardware allows reading out at twice this speed.

2.2. The quad module design and assembly

In order to cover large areas, the quad module shown in figure 1 was developed. Because of the complexity of the GridPix technology and the fragility of the grids, a small number of four chips per module was chosen. The chips are mounted on a common cooled base plate (COCA). They are electrically connected by wire bonds to a 6 mm wide PCB between the two pairs of chips. This allows the control and output lines to be directed to the backside of the quad to maximize the sensitive detection area. A short Kapton cable at the other side of the wire bond PCB provides a low impedance connection to the low voltage (LV) regulator. The grids are connected by $80\ \mu\text{m}$ insulated copper wires to a high voltage (HV) filtering board. The connection to the common HV input uses a $100\ \text{M}\Omega$ resistor for each grid to rapidly quench a micro-discharge. To support and cool the LV regulator board and the HV filtering board, a U-shaped

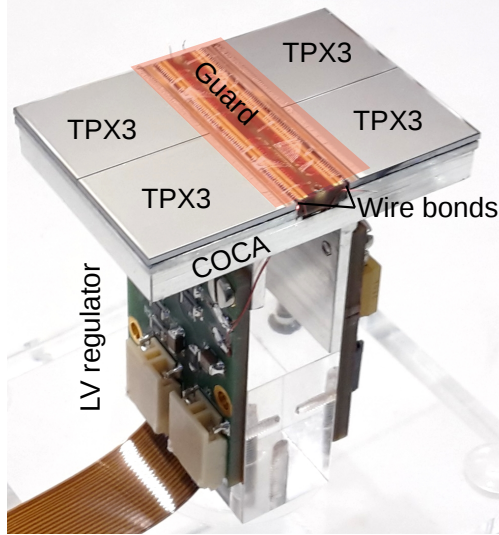


Figure 1: Picture of the quad detector with four Timepix3 GridPixes (TPX3) mounted on a cold carrier plate (COCA). The central guard was omitted to show the wire bond PCB, and its operating position is indicated with a transparent rectangle. On the left the Low Voltage (LV) regulator and flexible Kapton cable are visible.

54 support is attached by thermally conductive glue under the carrier plate. Fi-
 56 nally, the wire bonds of the quad are covered by a 10 mm wide central guard
 electrode located 1.1 mm above the grids to maintain a homogeneous drift field.

58 The external quad dimensions are $39.6\text{ mm} \times 28.38\text{ mm}$ of which 68.9% is
 active. In the present design the support components are made of aluminium
 contributing substantially to the material budget. In the future the material
 60 budget can be further minimized by replacing the aluminium by carbon based
 materials. During low rate operation, the module consumes 8 W of power of
 62 which 2 W in the LV regulator.

2.3. The quad detector

64 The quad module was embedded in a TPC consisting of a steel box and a
 40 mm high field cage to provide a homogeneous drift field. The sides of the
 66 field cage are formed by $75\ \mu\text{m}$ CuBe wires with a 2 mm pitch to facilitate UV
 laser beam measurements. The field cage is terminated by on one end the quad
 68 module fitted in a closely surrounding coppered frame at the grid potential,
 and on the other end a solid cathode plate. The whole structure was put in a
 70 gas-tight container with $50\ \mu\text{m}$ Kapton windows on two sides to minimize the
 material traversed by the beam.

72 3. Test beam measurement

The device was tested in October 2018 at the ELSA test beam facility in
74 Bonn. The ELSA accelerator provided 2.5 GeV electrons at a rate of approxi-
mately 10 kHz during spills of 16.0 s in beam cycles of 17.1 s. The whole quad
76 detector was mounted on a remotely controlled slider stage. To provide a pre-
cise reference track, the quad TPC was sandwiched between 2×3 planes of a
78 Mimosa26 telescope [7], see figure 2. Each plane consists of a MAPS detector
with 1152×576 pixels of size $18.4 \mu\text{m} \times 18.4 \mu\text{m}$.

80 A scintillator provided a trigger signal to the Trigger Logic Unit (TLU) [8]
which numbers the triggers and subsequently directs them to both the SPIDR
82 and telescope readout. The telescope hits were collected in time frames of
115.2 μs . Due to the high beam intensity, the telescope frames often contain
84 hits from more than one track. The Timepix3 was operated in data driven
mode with the trigger data merged in.

86 Because of the chosen limited link speed between the Timepix3 chips and
the SPIDR a maximum of 1.3 MHits/s could be read out. This caused some
88 hits to arrive late at the SPIDR readout, acquiring a wrong 409.6 μs course
timestamp. As a work-around hits, up to 200 timestamps of 409.6 μs after the
90 trigger were collected and analysed. The first track hit had to arrive no more
than 5 timestamps late, and the average course timestamp should not deviate
92 more than 150 timestamps.

During data taking the 700 ml gas volume was flushed at a rate of 16.7 ml/min
94 with premixed T2K TPC gas. This gas is a mixture consisting of 95 % Ar, 3 %
CF₄, and 2 % iC₄H₁₀ suitable for large TPCs because of the relatively large
96 drift velocity and the low diffusion in a magnetic field. The temperature and
pressure were relatively stable at 300.5 K and 1011 mbar. The gas mixture con-
98 tained a 814 ppm O₂ contamination and a 6000 ppm H₂O contamination, due
to the limited gas tightness of some of the materials for these molecules.

100 The cathode and guard voltages were set such that the electric field was
400 V/cm, which is close to the maximum drift velocity for the contaminated
102 gas. The grid voltage was set to 330 V, at which there is limited secondary
emission from the grid by UV photons produced in avalanches. The threshold
104 level being a trade off between noise, sensitivity and time walk, was set to about
550 e⁻. Some of the relevant run parameters are summarized in table 1.

106 4. Track reconstruction and event selection

4.1. Track reconstruction procedure

108 Tracks are reconstructed as straight lines. The y -axis is defined roughly
in the direction of the beam, and the x -axis and z -axis are in the horizontal
110 and vertical direction respectively. For the telescope, the y -coordinate is taken
from the plane position, and the x -coordinate and z -coordinate correspond to
112 the columns and rows. Apart from a small rotation, the x and y -coordinates
correspond to the columns and rows of the GridPixes. The z -coordinate is the
114 drift length calculated from the ToA and the drift velocity. Tracks are fitted

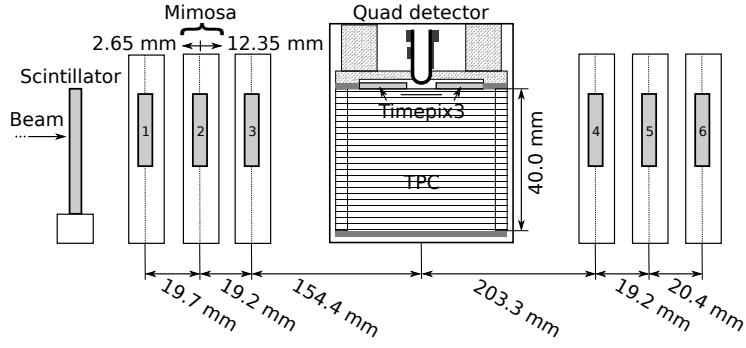


Figure 2: Setup of the quad with telescope at the ELSA test beam facility.

Table 1: Parameters of the three analyzed runs. The error on the temperature and pressure indicates the spread in the time the three runs were taken.

Runs duration	10 minutes
Triggers per run	2.2×10^6 triggers
V_{grid}	330 V
E_{drift}	400 V/cm
Threshold	$550 e^-$
Temperature	(300.5 ± 0.13) K
Pressure	(1011 ± 0.16) mbar
Oxygen concentration	814 ppm
Water vapor concentration	6000 ppm

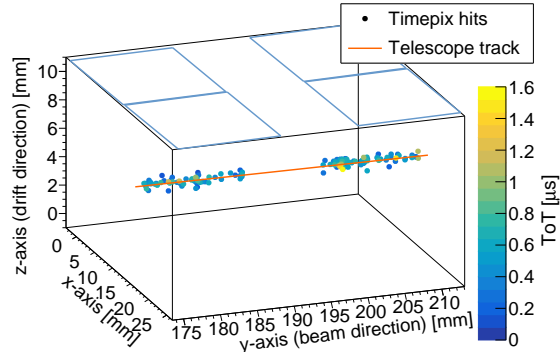


Figure 3: An event with 148 quad detector hits and the corresponding telescope track. The positions of the chips are outlined in blue.

using a linear regression fit with hit errors in the two directions perpendicular to the beam σ_x and σ_z . The expressions for the error values are given in sections 5.4 and 5.5.

The detectors are aligned using the data. First, the telescope is independently aligned. The positions in the y -direction along the beam are measured and kept fixed. Taking one plane as a reference, the other five planes can be rotated. These rotations and additionally two shifts in x -direction and z -direction for four of the planes are iteratively determined from the fitted tracks. Next, the quad detector is aligned. Using iterative alignment each chip has three rotations and two shifts in the x and z -directions. Additionally, each chip has one parameter describing the angle in the xz -plane between the drift direction and the pixel plane.

An example event with a telescope track is shown in figure 3.

4.2. Selections

In the telescope a stringent selection is made to acquire a sample of clean tracks. At least 5 planes should have a hit and the hits should be within $50 \mu\text{m}$ from the track. By requiring the slope difference of the track in the first three planes and in the last three planes to be smaller than 1 mrad, scattered tracks are rejected.

GridPix hits are considered if their ToA is within 500 ns of a trigger and their ToT is at least $0.15 \mu\text{s}$. The hits are collected using a track detected by the telescope as a seed. Outliers are rejected by requiring the residuals r (pulls r/σ) with respect to the telescope track to be smaller than 1.5 mm (2.0) in the x -direction and 2.0 mm (3.0) in the z -direction.

A track is rejected if it has less than 20 hits. Moreover the average position of all Gridpix hits must be within 0.3 mm in the x -direction and z -direction of the telescope track. Given the high beam rate, the TPC often contains multiple tracks overlapping in time. To suppress overlapping tracks and to reject tracks

Table 2: Table with selection cuts

Telescope
Number of planes hits ≥ 5
Reject outliers ($r_{x,z} < 50 \mu\text{m}$)
Slope difference between sets of planes $< 1 \text{ mrad}$
GridPix hit selection
$-500 \text{ ns} < t_{\text{hit}} - t_{\text{trigger}} < 500 \text{ ns}$
Hit ToT $> 0.15 \mu\text{s}$
Reject outliers ($r_x < 1.5 \text{ mm}, r_z < 2 \text{ mm}$)
Reject outliers ($r_x < 2\sigma_x, r_z < 3\sigma_z$)
Event Selection
$N_{\text{hits}} \geq 20$
$(N_{r_x < 1.5 \text{ mm}} / N_{r_x < 5 \text{ mm}}) > 0.8$
$ x_{\text{Timepix}} - x_{\text{telescope}} < 0.3 \text{ mm}$
$ z_{\text{Timepix}} - z_{\text{telescope}} < 0.3 \text{ mm}$

with delta electrons, 80% of the hits within 5 mm of a track are required to lie
 144 within a distance of 1.5 mm.

The selections are summarized in table 2 and the total efficiency for events
 146 is about 12%. Most events are rejected, because there are less than 20 GridPix
 hits corresponding to the telescope track.

148 5. Results

5.1. Number of hits

150 The distribution of the number of track hits per chip and the total number
 of track hits are shown in figure 4. The most probable number of hits per chip
 152 varies between 52 and 65 hits, and the mean varies between 65 and 80 hits.
 The most probable number of hits per quad is 131 and the mean number of
 154 track hits is 146 for an effective track length of approximately 27.5 mm. This is
 significantly below the calculated most probable value of 225 electron-ion pairs
 156 for a 2.5 GeV electron with this track length [9]. This is due to the too low
 effective grid voltage and possibly due to read out problems. Because of the low
 158 single electron efficiency, no energy loss (dE/dx) results were extracted.

5.2. Hit time corrections

160 To increase precision in the drift direction, the hit times were corrected. To
 correct for the double column structure and power distribution deformations
 162 of the Timepix3 chip, a ToT factor per column was acquired by injecting test
 pulses for each pixel. Furthermore, a ToA correction offset was determined from
 164 the test beam data based on the underlying substructure of 16×2 pixels due

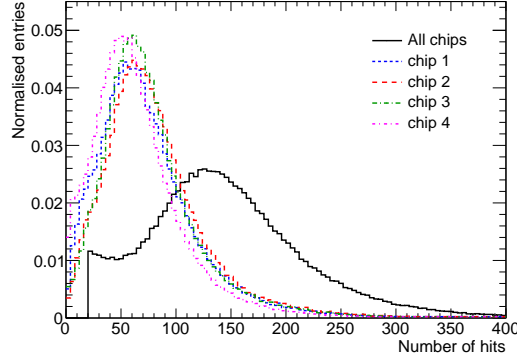


Figure 4: Distribution of the number of hits after track selection in total and per chip.

to the clock distribution. In addition one ToA correction offset per column and
 166 one offset per row was applied.

5.3. Time walk correction

168 A hit is registered when the collected charge reaches the threshold. Since it
 takes longer for a small signal to reach the threshold than it does for a large
 170 signal, the measured ToA depends on the magnitude of the signal. This effect
 is called time walk and can be corrected for by using the ToT as a measure of
 172 signal magnitude. In figure 5 the mean of z -residuals is shown as a function
 of the ToT for all four chips. The relation can be parametrized using the time
 174 walk δz_{tw} as a function of the ToT t_{ToT} :

$$\delta z_{\text{tw}} = \frac{c_1}{t_{\text{ToT}} + t_0}, \quad (1)$$

where c_1 and t_0 are constants determined from a fit per chip.

5.4. Hit resolution in the pixel plane

176 The resolution of the single electrons in the transverse plane (xy) was mea-
 178 sured as a function of the predicted drift position (z). Figure 6 displays this
 relation for tracks crossing a fiducial region in the center of the chip. The
 180 resolution for the detection of ionisation electrons σ_x is given by:

$$\sigma_x^2 = \frac{d_{\text{pixel}}^2}{12} + D_T^2(z - z_0), \quad (2)$$

where d_{pixel} is the pixel pitch size, z_0 is the position of the grid, and D_T is the
 182 transverse diffusion coefficient. The resolution at zero drift distance $d_{\text{pixel}}/\sqrt{12}$
 was fixed to $15.9 \mu\text{m}$. Tracks with a z -position around 0.5 mm are given a larger
 184 error because they scatter on the central guard. Fitting expression (2) to the
 data gives a transverse diffusion coefficient D_T of $398 \mu\text{m}/\sqrt{\text{cm}}$. The measured

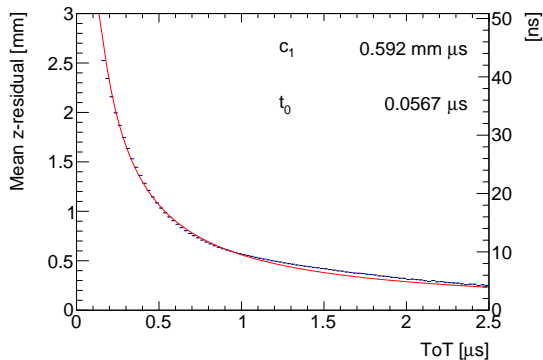


Figure 5: Mean z-residual without time walk correction as function of ToT, fitted with equation (1). The right axis is given in units of ns using the measured drift velocity of $54.6 \mu\text{m}/\text{ns}$.

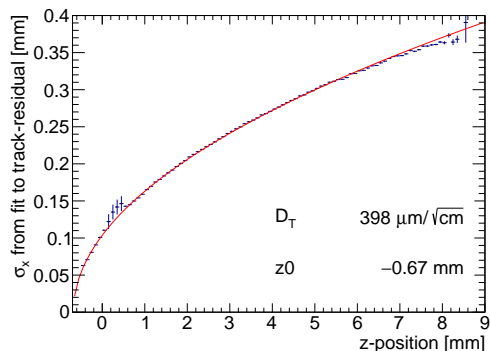


Figure 6: Measured hit resolution in the pixel plane (blue points) fitted with the resolution function according to equation (2) (red line).

186 value is larger than the value of $270 \mu\text{m}/\sqrt{\text{cm}}$ predicted by the gas simulation
 188 software Magboltz [10]. Probably this is due to an inaccuracy in the gas mixing,
 which caused the CF_4 content to be lower than intended.

To compare the precision of the GridPix readout with the precision of con-
 190 ventional pad based TPC readouts, the resolution can be calculated over the
 length of one pad row. For example, at a drift distance of 4 mm the resolution
 192 of a single ionisation electron is approximately $250 \mu\text{m}$, so the resolution of a
 6 mm track segment which has on average 32 electrons is therefore about $44 \mu\text{m}$.

194 5.5. Hit resolution in the drift direction

The measured z-position is directly related to the drift velocity. Using the
 196 predicted positions from the telescope, the drift velocity is measured to be

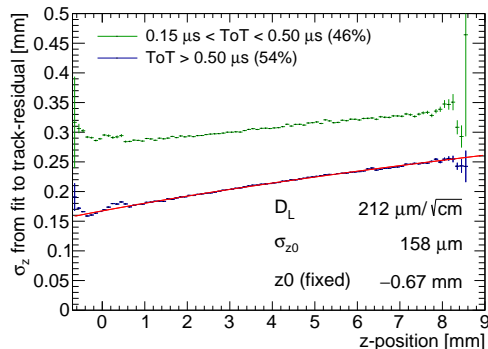


Figure 7: Measured hit resolution in drift direction split by ToT. The hits with a ToT above $0.50 \mu\text{s}$ (blue points) are fitted with the resolution according to equation (3) (red line). In the legend the fractions of hits in both selections are given.

54.6 $\mu\text{m}/\text{ns}$, which is slightly lower than the value of 59 $\mu\text{m}/\text{ns}$ expected by Magboltz [10].

The resolution for the detection of ionisation electrons σ_z is given by:

$$\sigma_z^2 = \sigma_{z0}^2 + D_L^2(z - z_0), \quad (3)$$

where σ_{z0} is the resolution at zero drift distance. The resolution as function of the drift distance is shown in figure 7 for tracks crossing the fiducial region. The longitudinal diffusion coefficient D_L was determined to be $212 \mu\text{m}/\sqrt{\text{cm}}$, which is equal to the value expected from a Magboltz calculation [10].

5.6. Deformations in the pixel plane

It is important to measure possible deformations in the pixel plane (xy), because for applications in a TPC this affects the momentum resolution. Because of limited statistics, the mean transverse (x) residuals are calculated in bins of 4×4 pixels over the quad plane using the tracks defined by the telescope, see figure 8. Only bins with more than 800 entries are shown.

A distortion is present near the edges of the chips. The cause is twofold; firstly there is a geometrical bias at the edge of the detector because only part of the ionisation cloud can be detected. Secondly, the grounded region at the edge of the Timepix3 die causes a non-uniformity of the electric field.

An empirically selected function of four Cauchy (Breit-Wigner) functions can be fitted to the geometrical bias and the non-uniformity of the field. Near the the top and bottom edges the size of the deformations is different, as such - while keeping the other parameters fixed - a 4th order polynomial function in y was fitted in a second step to set the scale. All in all, the fitted function is given by:

$$\delta x_{\text{deformations}} = \sum_{j=0}^4 \left(\frac{1}{\pi} \frac{\gamma_j}{(x - d_j)^2 + \gamma_j^2} \sum_{i=0}^4 (c_{ij} y^i) \right), \quad (4)$$

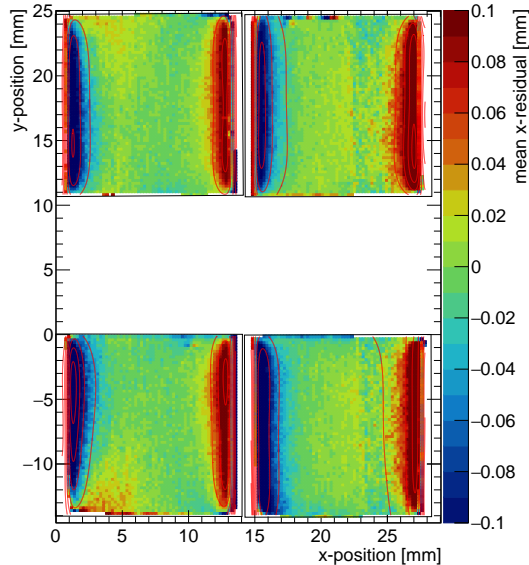


Figure 8: Mean residuals in the pixel plane (x -residuals) at the expected hit position, fitted with equation (4) (red contours).

220 where d_j and γ_j are the location and scale parameters of the Cauchy distribu-
 221 tions. c_{ij} are the parameters of the fourth order polynomial.

222 The outlines of the fitted function are shown in figure 8. The fitted function
 223 can be used as a correction by subtracting it from the mean residuals. The
 224 result of this procedure is shown in figure 9.

225 The r.m.s. of the distribution of the measured mean residual over the surface
 226 - or the systematic error for a measurement before the correction in the quad
 227 plane - is $31 \mu\text{m}$. After subtraction of the fitted correction function (4), the
 228 r.m.s. of the mean values is $13 \mu\text{m}$ over the whole plane and $9 \mu\text{m}$ in the selected
 229 region 2 mm from the edges indicated by a black outline. The distribution of
 230 the mean x -residuals after correction are shown in figure 10. The distortions
 231 could be further reduced by improving the homogeneity of the electric field near
 232 the dyke e.g. by adding a field wire above the quad detector at the boundaries
 between the neighbouring chips.

234 5.7. Deformations in the drift direction

235 A similar measurement is done for distortions in the drift direction. In figure
 236 11 the mean longitudinal (z) residuals are shown in bins of 4×4 pixels over the
 237 quad plane using the tracks defined by the telescope. Only bins with more
 238 than 800 entries are shown. As shown in figure 10, the r.m.s. of the distortion
 239 is $19 \mu\text{m}$ (0.35 ns) and $14 \mu\text{m}$ (0.26 ns) in the black outlined central area 2 mm
 240 from the edges.

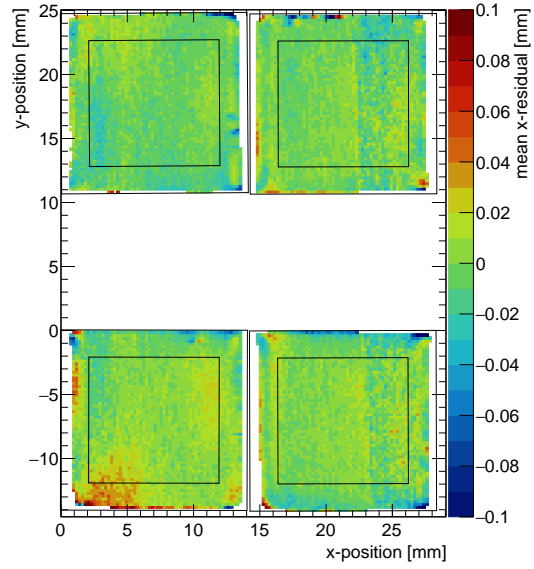


Figure 9: mean residuals in the pixel plane (x -residuals) at the expected hit position after subtracting the fitted edge deformations using equation (4).

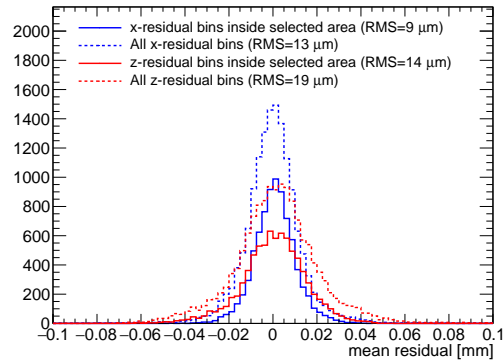


Figure 10: Distribution of the mean residuals from 4×4 bins in figure 9 (x -residuals) and figure 11 (z -residuals)

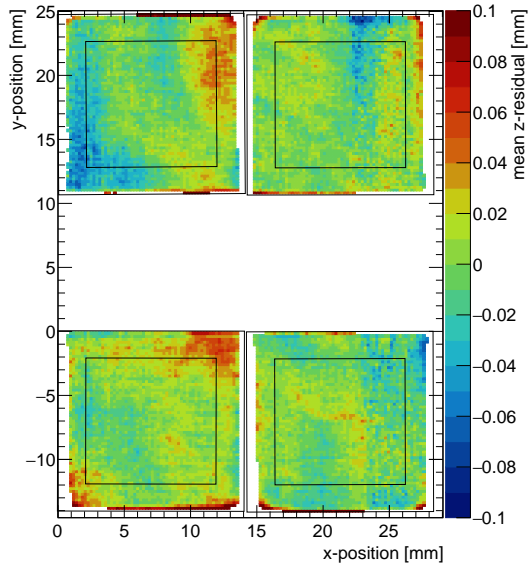


Figure 11: Mean residuals in the drift direction (z -residuals) at the expected hit position.

5.8. Quad detector resolution

242 The overall accuracy of a track position measurement using the quad de-
 243 tector can be tested by comparing the quad track to the telescope track. The
 244 difference will be a combination of statistical errors, systematic errors and mul-
 245 tiple scattering contributions. Here it is important to estimate the systematic
 246 error, because multiple scattering occurs primarily outside the fiducial gas vol-
 247 ume, and in applications with multiple quad modules the statistical errors will
 248 be further reduced.

Figure 12 displays the difference between the mean position of all quad
 250 track hits and the telescope track. The distribution has long tails, which are
 251 in part from unrelated background tracks that are erroneously matched. The
 252 number of background tracks is estimated by shifting the telescope timing by
 253 1000 frames and is shown for comparison. In fits, these tracks are accounted for
 254 by introducing a constant offset.

A fit with a Gaussian function with constant offset yields a standard deviation
 256 σ_x^{quad} of $41 \mu\text{m}$. This value is the result of various contributions. Firstly,
 257 the statistical precision of a position measurement is acquired from a track fit
 258 of the quad hits with hit errors. The statistical precision of the position at
 259 the center of the quad is $25 \mu\text{m}$. Furthermore, there is a systematic deviation
 260 of $9 \mu\text{m}$ in the pixel plane after the correction as discussed in section 5.6, and
 261 an additional systematic deviation in the x -direction of $17 \mu\text{m}$ along the drift
 262 direction. The latter is most likely due to electric field inhomogeneities.

In addition, the precision of the telescope is limited due to multiple scattering

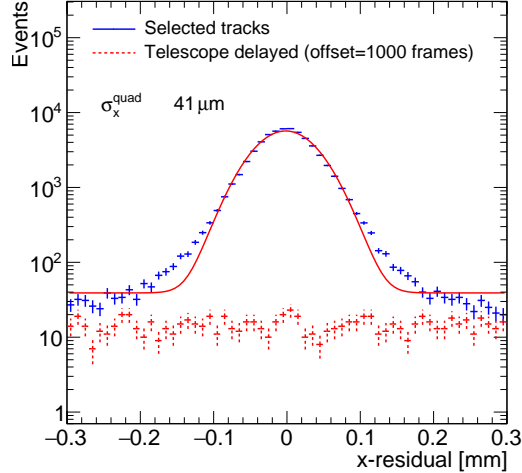


Figure 12: difference between mean hit position and track prediction in the pixel plane, fitted with a Gaussian plus a flat background (solid red line). In comparison the background tracks are shown (dashed red), acquired by offsetting the telescope by 1000 frames.

264 in the setup. The precision was calculated with a simple simulation of the setup
 265 using the approach to multiple scattering suggested by reference [11]. The setup
 266 has multiple scattering contributions from the telescope planes (0.075% X_0 per
 267 plane) [12], the air (0.084% X_0), the TPC gas (0.09% X_0) and the two Kapton
 268 foils (0.035% X_0) [11]. By comparing the track angle in the first three telescope
 269 planes and the second three telescope planes, the total radiation length of the
 270 setup is estimated to be 0.82% X_0 (0.66% X_0 expected). From the simulation
 the telescope precision at the quad is estimated to be 22 μm .

272 An overview of the contributing errors is given in table 3. In the end, there
 is still a small unidentified systematic error of 14 μm .

Table 3: Overview of the errors on the difference between mean hit position and track prediction in the pixel plane

Observed standard deviation σ_x^{quad}	41 μm
Statistical quad detector error	25 μm
Statistical telescope error	2 μm
Systematics over the pixel plane (corrected)	9 μm
Systematics along the drift direction	17 μm
Multiple scattering contribution	22 μm
Remaining systematic error	14 μm

274 6. Conclusion and outlook

276 A quad module with four Timepix3 based GridPixes has been designed and
realised. The module has dimensions of $39.6\text{ mm} \times 28.38\text{ mm}$ and an active
278 surface of 68.9%. The quad module was embedded in a TPC detector and
operated at the ELSA test beam facility. The single electron resolutions in the
280 transverse and longitudinal planes are similar to the results obtained for the
single-chip detector [5] and primarily limited by diffusion. It is shown that a
systematic error from the quad detector for the distortions over the pixel plane
282 of $13\text{ }\mu\text{m}$ ($9\text{ }\mu\text{m}$ in the central region) has been achieved. The demonstrated
resolution of the setup is $41\text{ }\mu\text{m}$, of which the statistical error is $25\text{ }\mu\text{m}$, the error
284 caused by multiple scattering in the setup is $22\text{ }\mu\text{m}$ and the total systematic
error is $24\text{ }\mu\text{m}$.

286 The next step is to demonstrate a large detection area with the quad module
as a building block and confirm the potential of the GridPix technology for large
288 detectors. A new detector with 8 quad modules carrying a total of 32 Timepix3
Gridpix chips is under construction.

290 Acknowledgements

This research was funded by the Netherlands Organisation for Scientific Re-
292 search NWO. The authors want to thank the support of the mechanical and
electronics departments at Nikhef and the accelerator group at the ELSA facil-
294 ity in Bonn. Their gratitude is extended to the Bonn SiLab group for providing
the beam telescope.

296 References

- 298 [1] P. Colas, A. P. Colijn, A. Fornaini, Y. Giomataris, H. van der Graaf,
E. H. M. Heijne, X. Llopart, J. Schmitz, J. Timmermans, J. L. Visschers,
300 The readout of a GEM- or micromegas-equipped TPC by means of the
Medipix2 CMOS sensor as direct anode, Nucl. Instrum. Meth. A535 (2004)
506–510. doi:10.1016/j.nima.2004.07.180.
- 302 [2] M. Campbell, et al., The Detection of single electrons by means of a
micromegas-covered MediPix2 pixel CMOS readout circuit, Nucl. Instrum.
304 Meth. A540 (2005) 295–304. arXiv:physics/0409048, doi:10.1016/j.
nima.2004.11.036.
- 306 [3] J. Kaminski, Y. Bilevych, K. Desch, C. Krieger, M. Lupberger, GridPix de-
tectors - introduction and applications, Nucl. Instrum. Meth. A845 (2017)
308 233–235. doi:10.1016/j.nima.2016.05.134.
- 310 [4] T. Poikela, J. Plosila, T. Westerlund, M. Campbell, M. D. Gaspari,
X. Llopart, V. Gromov, R. Kluit, M. van Beuzekom, F. Zappon,
312 V. Zivkovic, C. Brezina, K. Desch, Y. Fu, A. Kruth, Timepix3: a 65k
channel hybrid pixel readout chip with simultaneous toa/tot and sparse

- readout, *Journal of Instrumentation* 9 (05) (2014) C05013.
314 URL <http://stacks.iop.org/1748-0221/9/i=05/a=C05013>
- [5] C. Ligtenberg, K. Heijhoff, Y. Bilevych, K. Desch, H. van der Graaf,
316 F. Hartjes, J. Kaminski, P. M. Kluit, G. Raven, T. Schiffer, J. Timmer-
318 mans, Performance of a GridPix detector based on the Timepix3 chip, *Nucl.*
*Instrum. Meth. A*908 (2018) 18–23. doi:10.1016/j.nima.2018.08.012.
- [6] C. Krieger, J. Kaminski, M. Lupberger, K. Desch, A GridPix-based X-
320 ray detector for the CAST experiment, *Nucl. Instrum. Meth. A*867 (2017)
101–107. doi:10.1016/j.nima.2017.04.007.
- [7] J. Visser, M. van Beuzekom, H. Boterenbrood, B. van der Heijden, J. I.
322 Muñoz, S. Kulis, B. Munneke, F. Schreuder, SPIDR: a read-out system for
324 Medipix3 & Timepix3, *Journal of Instrumentation* 10 (12) (2015) C12028.
doi:10.1088/1748-0221/10/12/C12028.
- [8] D. Cussans, Description of the JRA1 Trigger Logic Unit (TLU), v0.2c,
326 EUDET Collaboration (2009).
328 URL [https://www.eudet.org/e26/e28/e42441/e57298/
EUDET-MEMO-2009-04.pdf](https://www.eudet.org/e26/e28/e42441/e57298/EUDET-MEMO-2009-04.pdf)
- [9] R. Veenhof, Garfield - simulation of gaseous detectors, version 9, Reference
330 W5050 (1984-2010).
332 URL <https://garfield.web.cern.ch>
- [10] S. F. Biagi, Monte Carlo simulation of electron drift and diffusion in count-
334 ing gases under the influence of electric and magnetic fields, *Nucl. Instrum.*
*Meth. A*421 (1-2) (1999) 234–240. doi:10.1016/S0168-9002(98)01233-9.
- [11] C. Patrignani, et al., Review of Particle Physics, *Chin. Phys. C*40 (10)
336 (2016) 100001, section 33.3. doi:10.1088/1674-1137/40/10/100001.
- [12] H. Jansen, S. Spannagel, J. Behr, A. Bulgheroni, G. Claus, E. Corrin,
338 D. Cussans, J. Dreyling-Eschweiler, D. Eckstein, T. Eichhorn, M. Goffe,
340 I. M. Gregor, D. Haas, C. Muhl, H. Perrey, R. Peschke, P. Roloff, I. Ru-
342 binskiy, M. Winter, Performance of the eudet-type beam telescopes, *EPJ*
Techniques and Instrumentation 3 (1) (2016) 7. doi:10.1140/epjti/
s40485-016-0033-2.
344 URL <https://doi.org/10.1140/epjti/s40485-016-0033-2>